ENGINEERING

Glove-based sensors for multimodal monitoring of natural sweat

Mallika Bariya[1,2,3]*, Lu Li[1,2,3]*, Rahul Ghattamaneni[1], Christine Heera Ahn[1], Hnin Yin Yin Nyein[1,2,3], Li-Chia Tai[1,2,3], Ali Javey[1,2,3]†

Sweat sensors targeting exercise or chemically induced sweat have shown promise for noninvasive health monitoring. Natural thermoregulatory sweat is an attractive alternative as it can be accessed during routine and sedentary activity without impeding user lifestyles and potentially preserves correlations between sweat and blood biomarkers. We present simple glove-based sensors to accumulate natural sweat with minimal evaporation, capitalizing on high sweat gland densities to collect hundreds of microliters in just 30 min without active sweat stimulation. Sensing electrodes are patterned on nitrile gloves and finger cots for in situ detection of diverse biomarkers, including electrolytes and xenobiotics, and multiple gloves or cots are worn in sequence to track overarching analyte dynamics. Direct integration of sensors into gloves represents a simple and low-overhead scheme for natural sweat analysis, enabling sweat-based physiological monitoring to become practical and routine without requiring highly complex or miniaturized components for analyte collection and signal transduction.

INTRODUCTION

In recent years, a variety of sweat sensors have been developed to monitor biomarkers for athletic and health monitoring applications amid a wider movement to determine what noninvasively and continuously accessible biofluids, including tears and saliva, can indicate about the physiological state of the body (*1*–*15*). Common to these platforms is a need for active sweat stimulation, either through exercise, iontophoretic/chemical stimulation, or heat treatment. Outside of a controlled laboratory environment, active stimulation poses practical limitations for widespread and routine sweat sensor use. Not only is it inconvenient to have to exercise or enter a sauna to obtain sensor measurements, but this may also be physically impossible for certain user groups, including patients and the elderly. Local iontophoretic stimulation poses its own challenges, including decreased sweating rates after repeated current application and concerns regarding local skin burning. Practically, sweat sensors must be able to autonomously access sweat without damaging the skin and must be compatible with routine activity, giving physiological insights without impeding user lifestyles. Natural thermoregulatory sweating, or background sweat that individuals continually secrete to microregulate body temperature without active stimulation, is a much more promising method for noninvasive and convenient biomarker access (*16*). Sweat is naturally secreted even during sedentary or routine activities like sleeping, sitting, and walking. Secretion rates are typically relatively low (~0.1 nl/min per gland versus over 1 nl/min per gland for exercise) but involve large-area sweat generation that produces nontrivial volumes of sweat overall (*17*–*19*). Furthermore, lower sweat rates reduce dilution of secreted analytes, better preserving equilibrium correlations between biomarkers in the sweat gland and those in surrounding interstitial fluid or blood (*18*, *20*, *21*). In this way, natural sweat could potentially provide better insight into the molecular state of the body compared to actively stimulated sweat.

While reducing sensor size (and thereby sample volume requirements) is one way in which sweat analysis can be supported by natural sweating, other methods include targeting body regions with particularly high sweat gland densities and inhibiting evaporation—a particular concern for distributed and low-rate sweat generation. Here, we present glove-based sensing platforms to analyze sweat naturally secreted on the hands and fingers during sedentary or routine activity (Fig. 1A). The fingertips, palm, and back of hand have some of the highest sweat gland densities on the body and therefore present attractive sites for accessing natural sweat (*22*, *23*). Gloves made of moisture-impermeable nitrile efficiently accumulate natural sweat by markedly limiting evaporation (fig. S1), enabling hundreds of microliters to be collected within half an hour while at rest. These large volumes could be harnessed for traditional off-body sweat analysis, already constituting a much more efficient and convenient method of sweat collection compared to exercise or chemical stimulation. Going a step further, sensors can be directly functionalized onto the inner surfaces of nitrile gloves (Fig. 1B) and finger cots (Fig. 1C) to allow in situ natural sweat analysis of analytes, including ions, heavy metals, xenobiotics, and nutrients (Fig. 1, D and E), without the need for miniaturized sensors. By taking advantage of a familiar and easy-to-wear form factor, glove-based analytics prioritize user comfort and convenience, providing a promising route to making sweat sensing routine for real-world application.

Electrodes can be fabricated in versatile patterns and locations on the inner surfaces of nitrile gloves and finger cots by simply defining electrode areas using a shadow mask and then evaporating conductive electrode materials. As a demonstration, we pattern gold and bismuth electrodes on the glove surface contacting the back of the hand—a region with particularly high sweating rates—and functionalize them into electrochemical sensors for sweat alcohol, zinc, chloride, and pH (*24*). We similarly fabricate a three-electrode system within nitrile finger cots to be selective for vitamin C. We verify the mechanical robustness of these platforms against the strains of on-body wear and demonstrate them for representative natural sweat

[1]Department of Electrical Engineering and Computer Sciences, University of California, Berkeley, CA 94720, USA. [2]Berkeley Sensor and Actuator Center, University of California, Berkeley, CA 94720, USA. [3]Materials Sciences Division, Lawrence Berkeley National Laboratory, Berkeley, CA 94720, USA.
*These authors contributed equally to this work.
†Corresponding author. Email: ajavey@berkeley.edu

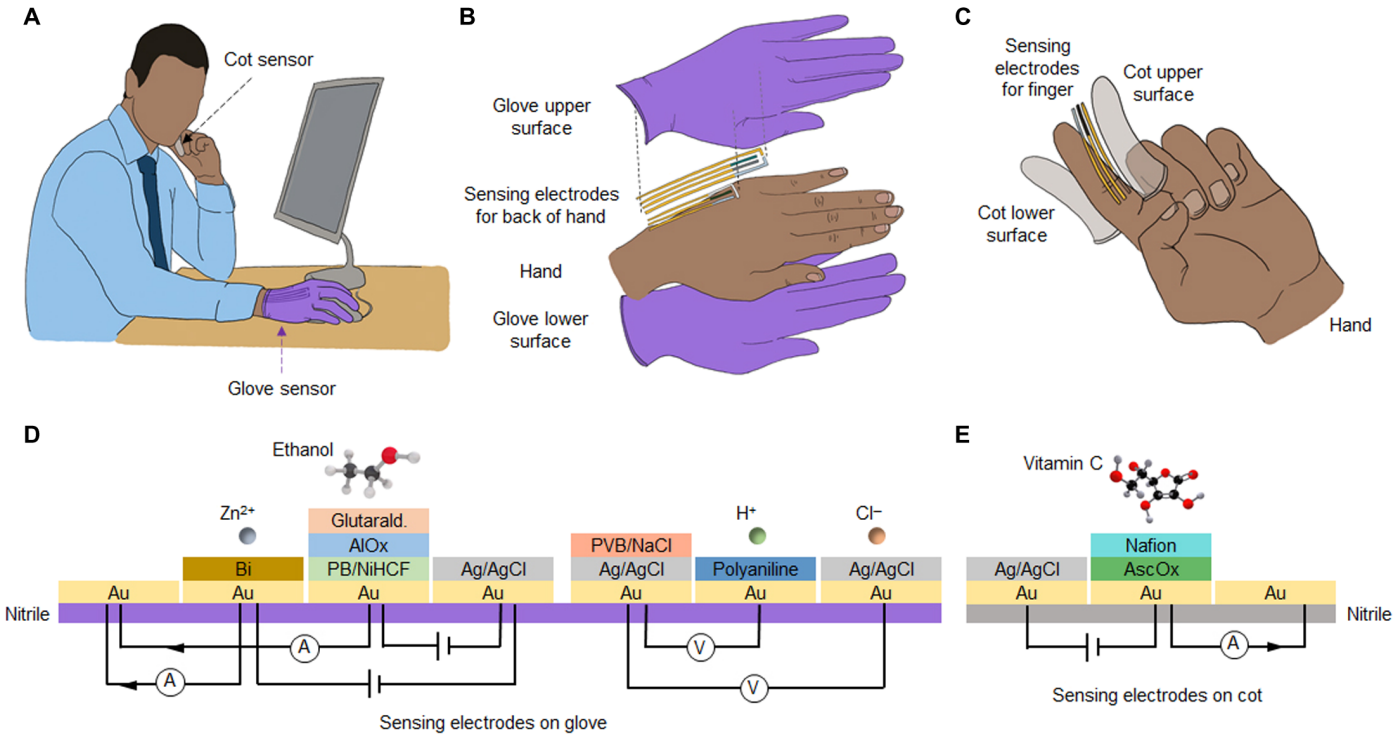

Fig. 1. Glove-based analytics for natural sweat analysis. (**A**) Glove-based sensors, including functionalized gloves and cots allow natural sweat analysis during sedentary and routine activity without active sweat stimulation. (**B**) Electrochemical sensors can be fabricated on versatile glove positions such as the back of the hand to target high sweat rate sites. The glove's nitrile material crucially protects against evaporation for rapid sweat accumulation. (**C**) Nitrile cots can be functionalized to target sweat gland-rich fingertips while offering a condensed form factor. (**D**) Cross-sectional schematic of the sensing layers and measurement schemes for zinc, ethanol, pH, and chloride sensors functionalized on a nitrile glove, and (**E**) vitamin C sensor functionalized on a nitrile cot.

monitoring applications, including using a sequence of gloves and cots to compare sweat and blood alcohol dynamics and to conduct multiday tracking of sweat vitamin C levels following vitamin supplement intake. In this way, we extract semicontinuous, dynamic information about sweat xenobiotics that are found to cohere with preexisting understandings of their metabolism and excretion in sweat, validating that each glove provides a faithful snapshot of sweat composition at that time. Single-point measurements obtained with individual gloves are therefore promising for rapidly gauging the physiological state of the body in applications where the presence of a chemical beyond a threshold level in sweat is noteworthy (such as for determining dangerous heavy metal exposure) or when a sweat analyte has an established correlation with blood (such as when monitoring alcohol levels). As these measurements can be obtained in just 30 min at rest, the functionalized gloves and cots present a valuable advantage over other sweat sensor systems that rely on exercise or chemical stimulation to access sweat or those that demand lengthy accumulation periods at low sweat rates. Overall, the presented sensors are found to be effective platforms for collecting and analyzing natural sweat during resting and routine activities, and relatively comfortable, inexpensive alternatives to the costly and invasive tests associated with traditional hospital-based monitoring of human health and physiological status.

RESULTS AND DISCUSSION

High sweat gland densities on the hand make it a promising site for sweat analysis compared to other body locations traditionally used for wearable sweat devices. Sweat gland densities are characterized for five subjects (two females and three males) on the index finger pad, palm, back of hand, wrist, forearm, forehead, and back of neck (Fig. 2A). Impressions of the glands are obtained using an iodine-soaked paper patch for the latter two regions to accommodate their firm yet curved skin surfaces, while the remaining regions are spotted with bromophenol dye to directly color the sweat glands, as discussed in Materials and Methods (*25*, *26*). Sweat glands are counted from these images for each subject and body site, revealing that the five subjects have average sweat gland densities of 441, 318, 290, 212, 171, 208, and 110 glands/cm^2 on the finger, palm, back of hand, wrist, forearm, forehead, and back of neck, respectively (Fig. 2B). The substantially higher densities on the hand surfaces cohere with previous findings and make them valuable target areas for sweat capture and analysis (*22*). By creating an enclosed region where secreted sweat is protected against evaporation, gloves and finger cots can capitalize on these high sweat gland density sites to rapidly accumulate sweat for analysis.

To characterize how much natural sweat is obtained for analysis with these platforms, subjects are recruited to wear nitrile gloves and cots during sedentary or routine activity at ambient temperatures. The volume of sweat accumulated after 30 min is identified by weighing the glove before being worn and after the 30 min of wear and calculating the difference. In addition, to capture any residual sweat left on the hand surface after glove removal, an absorptive pad is swiped across the hand immediately after glove removal and also weighed, faithfully recovering residual sweat to within a few microliters due to the rapid collection time under 1 min. This study is first

Fig. 2. Comparative sweat gland densities across body locations. (**A**) Sweat glands are imaged with bromophenol blue on the finger, palm, back of hand, wrist, and forearm. Sweat glands on the forehead and neck are imaged by imprinting onto iodine patches. Blue squares indicate locations of the sampled densities. Sweat gland images share the same scale. (**B**) Sweat gland densities are found by counting glands in the images from (A) across body sites for five subjects. A unique color is used for each subject. Photo credit: Mallika Bariya, University of California, Berkeley.

conducted for the nitrile glove platform (Fig. 3A). For 12 subjects (6 females and 6 males) sitting at ambient indoor workplace temperatures between 65°F and 70°F (approximately 18°C to 21°C) for half an hour, up to several hundreds of microliters of sweat is accumulated (Fig. 3B). The males produce an average of 475 μl of sweat on each hand, while the females produce an average of 180 μl of sweat on each hand, consistent with known biological differences (*27*). Since the nitrile gloves do not directly laminate the skin to suffocate any sweat glands and do not produce substantial local heating to raise core temperature or overcome the body's natural radiative and insensible evaporation mechanisms of heat loss, these large accumulated volumes are due to the body's natural thermoregulatory sweating process combined with low evaporation through the nitrile material (*28*, *29*). Similar volumetric secretion can be expected even without wearing gloves, but in this case, the exposed sweat rapidly evaporates and obscures the high volumes actually produced, leaving insufficient sweat for analysis. Creating an evaporation barrier is therefore a critical aspect of the glove-based sensing platform.

To more closely investigate factors that affect natural sweating rates, the influence of activity level and temperature is probed for a smaller subgroup of subjects. Six subjects (three females and three males) wear nitrile gloves for 30 min at ambient workplace temperature and at different activity levels, including sitting, standing, and light walking at under 75 steps per minute (Fig. 3C). Sweating rates, in general, are seen to increase with more strenuous activity, with some subjects nearly doubling their total secreted sweat volumes when standing compared to sitting. Next, activity level is kept fixed, while the temperature dependence of secreted sweat volume is studied for the six sitting subjects (Fig. 3D). Sweating rates generally increase with temperature, although more markedly for some subjects than others. The exact relationship between activity, ambient temperature, and accumulated sweat volume will depend on a host of other subject-dependent factors including body mass, hydration level, metabolic rate, etc., but overall, we find that for most subjects undergoing routine activity at ambient temperatures, large volumes of sweat in excess of 100 μl are available for natural sweat analysis within 30 min of glove-based accumulation (*30*).

Instead of wearing an entire glove, a nitrile cot worn on a single finger can provide an even less intrusive platform for natural sweat analysis while still accumulating substantial volumes of sweat due to the exceptionally high sweat gland densities on the fingers (Fig. 3E). To gauge how much sweat can be accumulated on each finger, four subjects (two females and two males) wear a cot on each finger for 30 min at ambient indoor temperature near 65°F (about 18°C) while sitting (Fig. 3F). Tens of microliters are secreted on each finger, with the thumb offering slightly higher volumes due to its larger surface area and the pinky secreting slightly less. Sweat contributions from the fingers constitute 30 to 50% of the overall sweat obtained from the hands of these subjects. These volumes are sufficient for sensing at least one biomarker without requiring miniaturized electrodes and indicate that any finger would be a suitable choice for natural sweat analysis.

Electrodes can be fabricated at diverse sites within the glove due to the simple shadow mask and evaporation-based patterning scheme, and can be customized to target any analyte of choice. While electrodes can be patterned to access the fingertips, palm, or multiple sites, for demonstration purposes, we fabricate sensors on the glove surface contacting the back of the hand (Fig. 4A) as this site is particularly immune to bending strains that might arise during hand motions. We create two demonstrative sets of electrochemical sensors—the first set executes xenobiotic sensing of alcohol and zinc using two working electrodes and shared reference and counter electrodes, while the second conducts electrolyte monitoring of sweat chloride and pH using two working electrodes and a shared reference. An alcohol sensor is included in the glove because sweat alcohol has been shown to correlate with blood alcohol concentration (BAC), potentially allowing the glove sensor to inform users of their body's alcohol absorption and warn against overdose (*10*, *31*). Zinc is targeted because heavy metals are commonly excreted in sweat, and while Zn is important for the immune system, it can be harmful when body levels are consistently elevated (*32*, *33*). Sweat chloride and pH can together indicate the body's acid/base balance and are further targeted to demonstrate that the glove sensor can support diverse electrochemical detection schemes (*34*, *35*). The xenobiotic array comprises four gold electrodes—two are functionalized with alcohol oxidase enzyme and bismuth metal, respectively, to target alcohol and zinc, one is an exposed gold counter electrode, and the last is developed into an Ag/AgCl reference electrode. The electrolyte array has three gold electrodes—one is coated in Ag/AgCl ink to target chloride ions, the second has electrodeposited polyaniline to measure pH, and the third becomes a polyvinyl butyral (PVB) reference electrode. Cross-sectional schematics of the functional layers are shown in Fig. 1D. The alcohol, Zn, pH, and chloride sensors fabricated

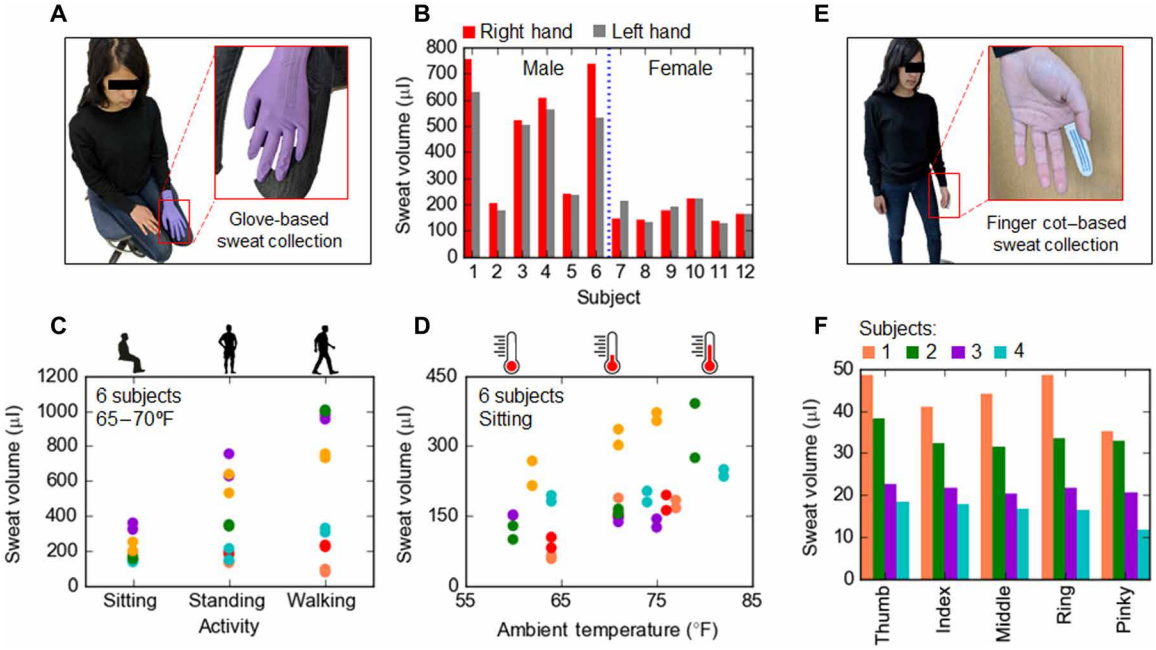

Fig. 3. Sweat volumes accumulated during routine activity. (**A**) Sweat accumulated in glove during 30 min of routine activity for (**B**) to (**D**). (B) Sweat collected from right (red) and left (gray) gloved hands for 12 subjects (6 male and 6 female) while sitting under ambient indoor conditions near 65°F. (C) Sweat accumulated from six subjects at different activity levels (three male and three female) shows a generally increasing sweat rate with activity level. (D) Sweat accumulated from six subjects over a range of ambient temperatures while sitting indicates a rough increase in sweat rate with temperature. (**E**) Sweat accumulated in finger cot for 30 min for (F). (**F**) Finger cots worn on each finger for four subjects (two males and two females, each designated a different color) show slightly higher sweat volume accumulated on the thumb and slightly lower volume on the pinky, roughly scaling with finger surface area. Photo credit: Lu Li, University of California, Berkeley.

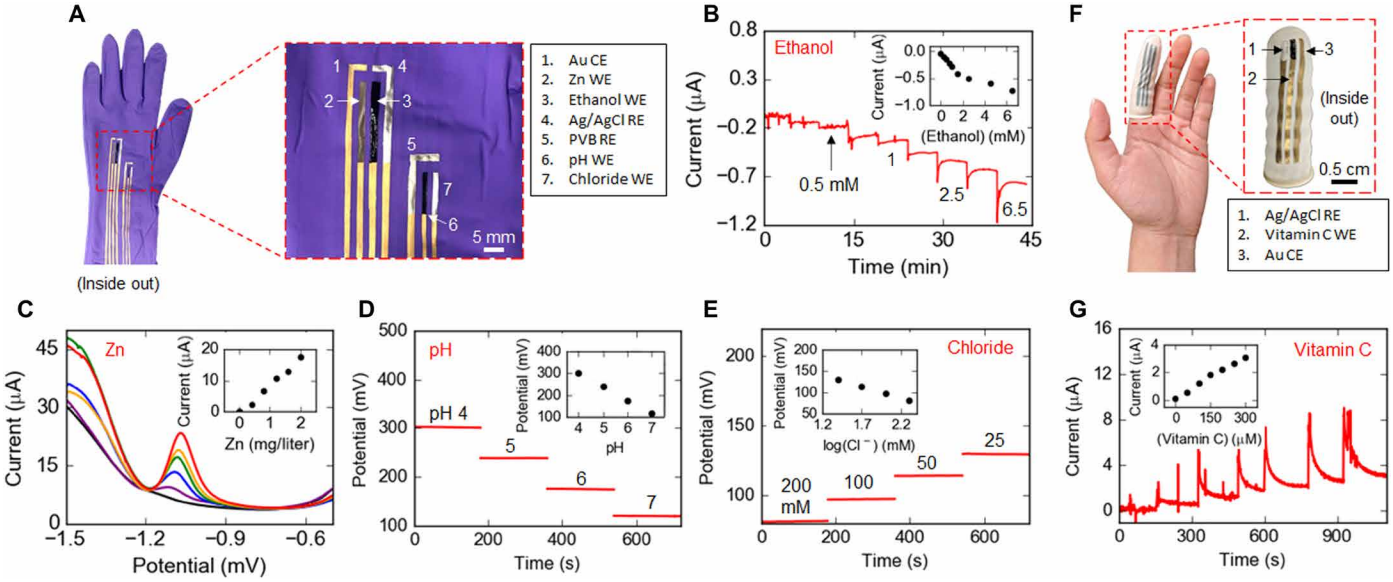

Fig. 4. Electrochemical characterization of glove-based sensors. (**A**) Gold electrodes are evaporated on the inner glove surface and functionalized with sensing layers to target zinc, ethanol, pH, and chloride ions in sweat. Calibration curves in buffer solutions of different analyte concentrations are shown for (**B**) ethanol, (**C**) Zn, (**D**) pH, and (**E**) chloride. (**F**) three-electrode system on the inside of a finger cot composed of evaporated gold functionalized with sensing materials to detect vitamin C. (**G**) Calibration curve of vitamin C sensor in buffer solutions. Photo credit: Lu Li, University of California, Berkeley.

on the glove are calibrated in Fig. 4 (B to E). The alcohol sensor is sequentially tested in 1× phosphate-buffered saline (PBS) buffer solutions of 0, 0.25, 0.5, 0.75, 1, 1.5, 2.5, 4.5, and 6.5 mM ethanol (Fig. 4B), with calibration curve inset, and shown to have an even wider range of sensitive detection in fig. S2 to accommodate expected sweat alcohol levels (*36*, *37*). The zinc sensor is tested in 0.001 M acetate buffer solutions of zinc (0, 400, 800, 1200, 1600, and 2000 μg/liter; Fig. 4C), giving a linear calibration curve. Note that the signal magnitudes

obtained from the alcohol and zinc sensors scale with working electrode area and are therefore subject to the particular geometry of the patterned electrodes. The pH sensor is sequentially tested in McIlvaine buffer solutions of pH 4, 5, 6, and 7, which encompass the typical pH range of sweat (Fig. 4D), giving a nearly ideal Nernstian sensitivity at 60.3 mV/pH. The chloride sensor is tested in 1× PBS buffer solutions at 25, 50, 100, and 200 mM NaCl, also giving a near-Nernstian sensitivity at an average of 15.9 mV per doubling in chloride concentration or 52.8 mV per decade (Fig. 4E). Overall, the performance of these sensors on the glove's soft, nitrile substrate is similar to what has been previously demonstrated by our group and others on more planar, rigid polyethylene terephthalate (PET) (*3*, *10*, *33*, *38*).

Given the smaller surface area available, a single three-electrode system for xenobiotic sensing of vitamin C is patterned on the nitrile cot to analyze natural sweat on the fingertips (Fig. 4F). The electrode heads are centered on the finger pad, a location that is relatively immune to strains associated with bending of the fingers. Vitamin C is chosen to target as its presence in sweat could indicate levels of daily intake or vitamin deficiency (*39*, *40*). This array has with three underlying gold electrodes—one is coated in Ag/AgCl ink to be the reference, the second is functionalized with ascorbate oxidase to interact with vitamin C, and the third is left as bare gold to act as the counter electrode. A cross-sectional schematic of the electrode layers is shown in Fig. 1E. This system's response to vitamin C concentrations between 0 and 300 μM in increments of 50 μM is linear and highly sensitive (Fig. 4G), with similar performance compared to our group's previous demonstrations on PET (*41*).

As the sensors' electrical signals are relayed through long electrode lines that end at the wrist of the glove or edge of the cot where a measurement system can be connected, it is important that the electrodes are mechanically robust when the glove-based platforms are worn. Specifically, the sensors' underlying electrodes must have recoverable conductivity or resistance values when the platforms are deformed during motion and wear, as deformation is expected to occur along the extended electrode length but not so much at the very head of the electrode where the sensing membranes are located. To characterize this electromechanical stability, we pattern an 8-cm-long electrode line on the nitrile substrate and calculate its resistance between 0 and 15% strain (Fig. 5A), a conservatively broad range given that strains during on-body wear are typically under 2% for electrodes contacting the back of the hand (as seen in fig. S3) (*42*). Note that resistance changes associated with deformation during insertion of the hand into the glove are ignored as this is a one-time operation that can be conducted carefully and introduces negligible baseline strains, and any residual resistance changes are accounted for during calibration after on-body testing. While the electrode deformation produces a change in resistance during strain, the resistance goes back to its original, prestrained value when relaxed back to 0% strain, as indicated by the red star. This highlights the recoverability of the system, indicating that the electrode does not crack or undergo permanent damage when stretched. This behavior arises because the nitrile glove is originally extended over the sample holder during gold evaporation, forming a percolating network of Au clusters or ligaments, rough surface features that connect over fine cracks to ensure electrical conductivity of the relaxed nitrile, as demonstrated previously for other thin metal films on elastomeric substrates (*43*, *44*). This structure is formed because of a large mismatch of thermal expansion coefficients of the elastomer and metal during evaporation. When the substrate is strained, the metal network accommodates by twisting or deflecting out of the plane but remains bonded to the soft substrate, effectively deforming elastically without fatigue and keeping the Au microstructure intact. Once the substrate is relaxed and strain withdrawn, the network of clusters returns to its original state, and the original electrical resistance of the electrode is recovered. Overall, contact between the clusters changes but does not sever under strain as the rough gold surface elastically deforms and recovers back to the original rough contact when the nitrile is relaxed. This explanation is supported by optical microscope images of the gold electrode layer before, during, and after 15% strain in fig. S4. Note that at rest, conductivity of the approximately 150-nm-thick evaporated Au film is measured to be around 8×10^5 S/m, around two orders lower than that of bulk Au, as expected for thin films. Resistance rather than conductivity values are reported for the electrode under deformation in Fig. 5 since information on the exact change in geometric structure of the electrode under deformation is not available. Furthermore, note that strains and resistance measurements are applied and obtained with the nitrile substrates in their final right-side-out configurations that match the state of functionalized gloves or cots ready for on-body wear, indicating that these platforms are mechanically robust for use.

To ensure that the electrode layer recovers even after numerous deformation cycles, the same electrode is put through 100 cycles of 2% strain, with resistance measured during the relaxed state after each cycle (Fig. 5B). The measured resistance values after 0, 1, 5, 10, 50, and 100 cycles are 180, 176, 180, 169, 193, and 193 ohms, respectively, essentially identical values given a variation of around ±10 ohms with the multimeter measurement system. Extended strain testing with more complex twisting and bending cycles and higher tensile strain bears this robustness out further in fig. S5.

While the electrode does not break under strain and recovers to its original state, the change in resistance during deformation seen in Fig. 5A could potentially causing noisy sensor signals when the hands or fingers are moved. To characterize how severe the change in resistance is from different types of deformation, we probe the electrode under relaxed, folded, twisted, and stretched (or 2% strained) states in Fig. 5C. The resistance recovers when the electrode is relaxed after each type of deformation, indicating mechanical robustness. Furthermore, strain is seen to most severely affect the electrode resistance. To gauge whether this change in electrode resistance affects the final sensor signal, we functionalize the electrode into a representative chloride sensor and calibrate it under relaxed and strained states (Fig. 5D), with a potentiometric sensor chosen for testing here since enzymatic sensors with nanotextured mediator layers have sensor signals limited by the amount and accessibility of enzyme, which quickly stabilizes under strain as studied in previous works (*45*–*47*). Figure 5D shows that strains on the order of those expected during routine hand motions (as quantified in fig. S3) do not have a substantial impact on the overall sensor response—for example, no noticeable shifts in overall potential occur during transitions from relaxed to strained states. This indicates that signal contributions from the sensing layers' interaction with the target analyte dominate over changes in the electrode wire resistance. Overall, these electromechanical tests highlight that the evaporated Au electrodes do not crack under the glove deformations typically undergone during on-body wear, have recoverable characteristics, and do not ultimately constitute a substantial source of noise in the glove sensor response.

Having established the electrochemical and electromechanical robustness of the glove-based sensing platforms, we next conduct

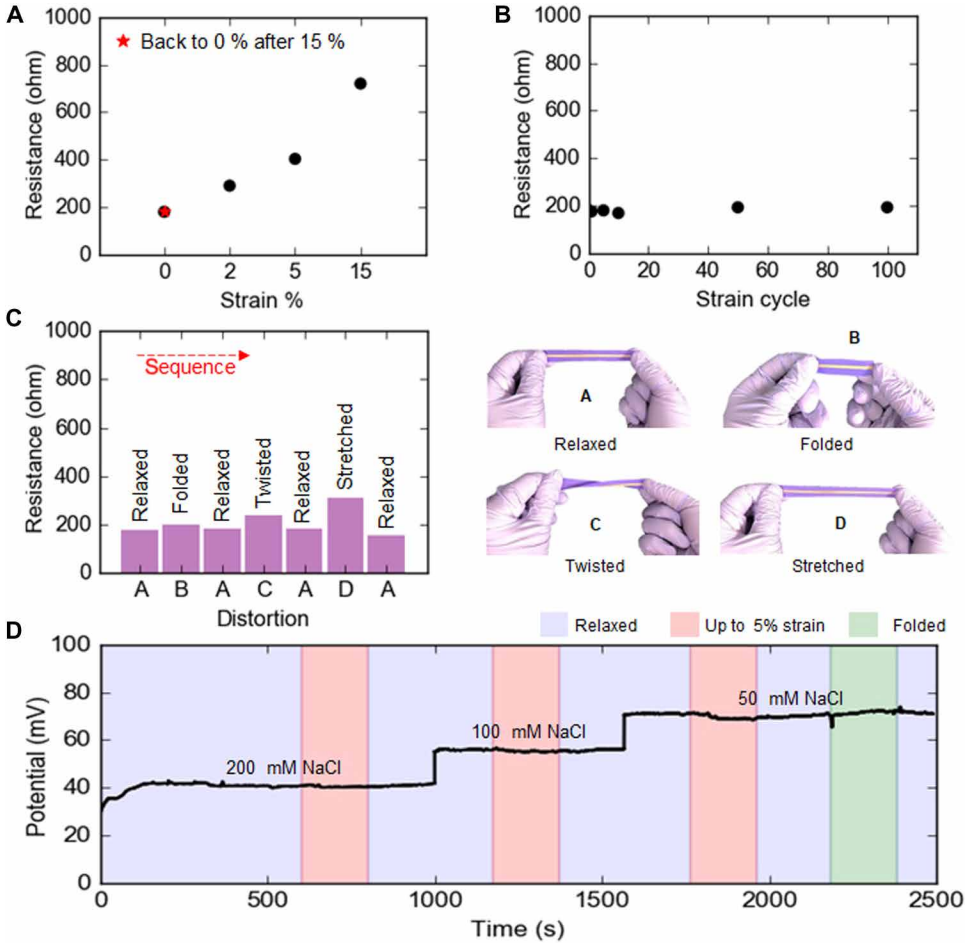

Fig. 5. Characterization of electrode robustness under mechanical deformation. (**A**) Resistance of an 8-cm evaporated Au electrode on the nitrile glove is measured between 0 and 15% strain. Red star shows relaxed electrode resistance once 15% strain is removed. (**B**) Resistance of the 8-cm electrode is measured at the relaxed state after 0, 1, 5, 10, 20, 50, and 100 cycles of 2% applied strain, showing that the electrode consistently recovers even after multiple distortions. (**C**) The electrode is exposed to a series of distortions, including folding, twisting, and stretching (via 2% strain). Stretching/strain has the most pronounced impact on the electrode resistance during the distortion, but the electrode closely recovers to the original resistance of its relaxed state after each deformation. (**D**) A representative chloride sensor on the glove is calibrated while strained and folded. The distortions do not substantially affect the sensor signal. Photo credit: Lu Li, University of California, Berkeley.

representative human subject trials for sweat alcohol and vitamin C monitoring to demonstrate the flexibility and versatility of glove-based analytics for natural sweat monitoring. In each trial, the subject wears a functionalized glove or cot platform for around 30 min at a time to accumulate sufficient natural sweat during sedentary or routine activity, with on-body measurements made at the end of this period once enough sweat is accumulated on the electrodes. Each glove or cot gives a single measurement that represents the average sweat analyte concentration over that 30-min interval, since sweat is continually accumulated and mixed during that time. By wearing multiple gloves or cots in sequence, the overarching dynamics of the target sweat analyte can be captured through single-glove snapshots of the sweat composition in time, allowing semi–real-time tracking of the overarching analyte dynamics. The first demonstrative trial tracks natural sweat ethanol content over 6 hours after a subject introduces alcohol into the body by drinking wine (Fig. 6A). A series of 10 gloves are used with around 30-min accumulation time per glove and 10 to 15 min in between to wipe down the hand and put on a fresh glove. In parallel, a breathalyzer is used to simultaneously track BAC levels for comparison. On the basis of the alcohol content of the wine, around 45 ml of alcohol is consumed in total over a 15-min period, ending at time demarcated 0 min [Fig. 6B(i)]. Following this intake, BAC level steeply rises to a maximum of 0.13 before slowly dropping over the next 6 hours [Fig. 6B(ii)]. With a delay of around 30 to 40 min compared to BAC levels, sweat alcohol content elevates to a maximum of 5.6 mM before tapering down to 2.1 mM at the end of this measurement period [Fig. 6B(iii)]. Integrity of these measurements is established via comparison of a subset of on-body and off-body sensor measurements in table S1. Note that each glove's sweat measurement marked by a red point in Fig. 6B(iii) is centered in the middle of the 30-min period of wear, since the measurement reflects the average sweat composition over that period. On the basis of the overarching trend, the sweat alcohol content is expected to keep decreasing toward the preintake level denoted by the first glove/red point. This sweat trend is similar to what has previously been reported, underscoring the effectiveness of the glove-based sensor for dynamic monitoring (*7*).

A second trial explores how natural sweat can provide insight into the body's adsorption and metabolism of vitamin C following supplement intake. A subject consumes 1000 mg of vitamin C dissolved

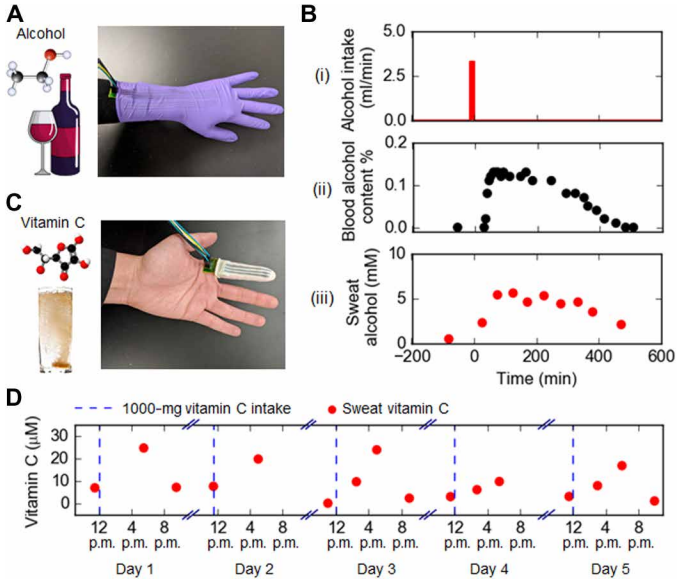

Fig. 6. On-body multiglove study of natural sweat analyte dynamics. (**A**) Subject introduces alcohol into the body by drinking wine, and subsequent excretion of alcohol in natural sweat is studied using the glove-based sensing platform. (**B**) Time 0 indicates when alcohol consumption is finished. (i) Alcohol intake versus time. (ii) BAC as measured by a breathalyzer. (iii) Natural sweat alcohol concentration is tracked over a 6-hour period using 10 gloves, with each glove providing an average alcohol concentration measurement for the 30-min time period over which it was worn. Each glove's measurement is indicated by a red point at the end of the 30-min interval. (**C**) Subject consumes 1000 mg of vitamin C dissolved in water each day for 5 days, and the resulting vitamin C that emerges in natural sweat is tracked using functionalized finger cots. (**D**) Natural sweat vitamin C concentration is plotted with red dots (each representing a measurement by one finger cot 30 min of accumulated sweat) over 5 days. Daily peaking behavior demonstrates the competing adsorption and metabolism mechanisms typical of xenobiotics in the body. Dashed blue lines indicate time of vitamin C intake. Photo credit: Lu Li, University of California, Berkeley.

in water at 12 p.m. each day for 5 days, and vitamin C concentration in subsequent naturally secreted sweat is measured using the functionalized finger cot platform (Fig. 6C). Each day, two to four finger cots are worn for 30 min at different time points, with the sweat measurement from each glove marked by a red point centered within its corresponding 30-min interval in Fig. 6D. As seen in Fig. 6D, sweat vitamin C content is lowest (less than 10 μM) right before intake (denoted by a vertical dashed blue line) and is elevated 4 to 5 hours later before dropping down overnight. This peaking trend is common of xenobiotics in the body, where concentrations originally rise as the chemical is absorbed before lowering as is it metabolized and removed from the system (*40*, *48*–*50*). Integrity of the on-body vitamin C measurements is borne out by comparing a set of on-body and off-body sample measurements in table S1. Note that more frequent finger cot application could be used to capture the exact vitamin C peaking point in sweat. Furthermore, note that sweat vitamin C levels seem to vary day to day, which could be due to variation in the subject's daily diet and hydration status amid other factors that affect physiological status.

While the alcohol and vitamin C trials demonstrate that glove-based analytics for dynamic monitoring of natural sweat biomarkers are an effective alternative to conventional hospital or home healthcare devices, these trials primarily validate the accuracy and reliability of this platform. The true advantage of glove-based sensors over other sweat sensing systems is how conveniently and rapidly they can be used for individual biomarker measurements. Rapid single-point assessment of physiological status could be done using just one glove or cot, as demonstrated by measuring the sweat pH and chloride levels of three subjects to gauge their acid/base balance in fig. S6. Overall, the glove-based sensing platforms are effective and versatile for natural sweat analysis, with simple electrode fabrication schemes that allow custom, application-specific sensors to be patterned and functionalized. To make electrode fabrication repeatable and scalable, stencils or laser-cut tape can be used in future to identically pattern electrodes on multiple gloves. Paper fluidics can be developed and incorporated in the gloves to gauge total secreted sweat volume and approximate sweat rate. Custom printed circuit boards (PCBs) or application-specific integrated circuit (ASIC) units can be developed to attach to the electrode stems near the wrist of the glove or base of the cot, enabling autonomous signal extraction that would further promote this platform for routine sweat analysis. Going forward, glove-based analytics represents a valuable tool for performing physiological and correlation studies on natural sweat to better understand how sweat analysis can be used to probe the health and state of the body.

CONCLUSION

We present wearable sweat sensors with convenient glove-based form factors for rapid accumulation of natural thermoregulatory sweat without active sweat stimulation. This platform enables sweat sensing under routine and even sedentary activity toward making sweat-based biomarker monitoring practical for daily life. By targeting high sweat gland densities on the hand and inhibiting evaporation, glove and finger cot sensors allow accumulation of hundreds of microliters of natural sweat under an hour of wear, eliminating the need for highly miniaturized sensors to access natural sweat. We functionalize representative electrochemical sensor on the inner glove surface and conduct on-body measurements to demonstrate the ease and simplicity of glove-based analytics for tracking xenobiotic dynamics in sweat. Functionalized gloves and cots support versatile electrode placement, are electromechanically robust under the strains of on-body wear, and retain the high level of performance typically associated with more rigid and planar substrates. Overall, the presented glove-based sensing platforms are an accessible, user-oriented approach to natural sweat analysis and can be adapted for versatile health and physiological monitoring applications.

MATERIALS AND METHODS

Materials

Bovine serum albumin, glutaraldehyde, alcohol oxidase solution (from *Pichia pastoris*), PVB resin BUTVAR B-98, sodium chloride (NaCl), potassium chloride (KCl), iron (III) chloride, potassium ferricyanide ($K_3Fe[(CN)_6]$), zinc standard AAS solution (1000 mg/liter in nitric acid), and aniline were purchased from Sigma-Aldrich. PBS was purchased from Thermo Fisher Scientific. Powder-free nitrile gloves and finger cots were purchased from manufacturers Kimberly-Clark and First Aid Only.

Fabrication of functionalized electrodes on the glove

A simple shadow mask is built and applied onto the glove's inside surface, keeping electrode areas open and covering the rest of the

glove. Electron beam evaporation is used to deposit 150-nm Au, followed by a similar taping and evaporation procedure to deposit 300-nm Bi on the head of the zinc working electrode. For the alcohol sensor, electrodeposition of Au nanodendrites is followed by cyclic voltammetry to deposit two interdigitated layers each of Prussian Blue mediator and nickel hexacyanoferrate (NiHCF) stabilizer, as demonstrated in previous work (*4*, *51*). For a working electrode area of approximately 8 mm^2, 6 μl of alcohol oxidase enzyme solution (6.5 parts BSA to 13.5 parts AlO_x) is dropcast followed by 3 μl of 0.02% glutaraldehyde solution and allowed to dry overnight (solution volumes are scaled with electrode area). The chloride sensor and Ag/AgCl reference electrode are fabricated by depositing Ag/AgCl conductive ink over the Au electrode heads, while the PVB reference involves deposition of a thick layer of PVB solution (saturated with NaCl) over Ag/AgCl ink, as demonstrated in our previous work (*3*). The pH sensor is fabricated by electrodepositing polyaniline similar to our previous work (*38*). Vitamin C working electrode is functionalized by electrodepositing a solution of 0.02 M 3,4-Ethylenedioxythiophene (EDOT) and 0.02 M $LiClO_4$for 1 min at 1.1 V versus Ag/AgCl reference. For an electrode area of roughly 8 mm^2, 5 μl of ascorbate (2.5 mg ml^{-1}) oxidase dissolved in 1× PBS buffer was dropcast onto the electrode surface followed by 4 μl of 0.5% Nafion solution, as demonstrated in our previous work (*41*). After electrochemical functionalization is complete, the glove or finger cot is turned right-side out before it is calibrated or used for on-body measurement. Note that this inverting process produces negligible change in the resistances of each electrode, as indicated in table S2.

Imaging sweat glands and characterizing their densities

Two methods were used to image sweat glands using bromophenol dye and iodine patches, respectively, as demonstrated in previous work (*25*, *26*). Bromophenol blue was dissolved in pure acetone in a 5% (w/v) solution and then mixed with silicone in 1:1 volumetric ratio. The mixture was magnetically stirred at 25°C until the acetone evaporated away and an orange solution was formed. The skin surface was washed and totally dried before the bromophenol dye was spread in a thin layer and allowed to react with moisture from the sweat gland, turning the orange dye blue in the sweat gland region within a few minutes. A photograph of the skin surface with a nearby ruler (for size calibration) was then captured for software analysis. The second method involved placing pads of paper in a sealed container (of roughly 1-liter volume) with <2 mg of solid iodine for 2 days, such that the paper was impregnated with iodine vapor. The pads were directly forced against the washed and dried skin surface for 5 s, transferring images of the sweat glands to the paper. A photograph of the iodine pad was then captured. Sweat gland density measurements were made by using ImageJ for both methods. A fast Fourier transform band-pass filter followed by thresholding was applied to each image to capture both small and large sweat glands in the analyzed area. The number of sweat glands was divided by the measurement area to give the sweat gland density. This process was repeated three times for each image and averaged to estimate the sweat gland density per body site.

Characterization of glove sensor response

Sensors fabricated on the glove electrodes were calibrated off-body using a sequence of buffer solutions prepared with known concentration. For chloride and pH sensor calibration, the sensors were conditioned in high-concentration analyte solution (200 mM NaCl and McIlvaine buffer of pH 4, respectively) for 10 min before beginning calibration via open-circuit voltage measurement, and 1 min of stabilization time was used between solutions. Alcohol and vitamin C sensor calibrations were conducted via chronoamperometry at an applied potential of 0 and 0.2 V, respectively. For Zn heavy metal sensing, square wave anodic stripping voltammetry was used with 30-s preconcentration at −1.5 V followed by stripping from −1.5 to −0.5 V.

On-body sweat analysis using the glove sensor

On-body human trials were carried out at the University of California, Berkeley, in compliance with the human research protocol (CPHS 2014-08-6636) approved by the Berkeley Institutional Review Board. Subjects washed their hands with soap and water and allowed them to totally dry before donning the glove sensors or finger cots. Glove sizes were chosen to comfortably fit the subjects' hands with a reasonable but not too tight seal near the wrist while ensuring a snug fit with good glove-to-skin contact. A paper pad was placed over the electrode heads to retain sweat cumulatively over the duration of wear and to electrochemically connect the working, reference, and counter systems without electrically contacting the skin. A protective barrier layer (Kapton or a 0.0005-inch-thick PET insert) was used to cover the long electrode lines to prevent shorting and direct skin contact. The ends of the electrodes near the wrist portion of the glove or base of the finger cots were connected to a Gamry and/or CH Instruments potentiostat for signal extraction. Sensor measurements were made once the glove had been worn for roughly 30 min to ensure accumulation of enough sweat to obtain reliable measurements. The sensors were calibrated before and after on-body data collection for accurate conversion of raw signals to concentration estimates. In future, calibration can be made more user-friendly by introducing manually activated valves to release calibration solution or by moving to automated fabrication to reduce intersensor variability.

SUPPLEMENTARY MATERIALS

Supplementary material for this article is available at http://advances.sciencemag.org/cgi/content/full/6/35/eabb8308/DC1

REFERENCES AND NOTES

1. J. Heikenfeld, A. Jajack, B. Feldman, S. W. Granger, S. Gaitonde, G. Begtrup, B. A. Katchman, Accessing analytes in biofluids for peripheral biochemical monitoring. *Nat. Biotechnol.* **37**, 407–419 (2019).
2. H. Lee, C. Song, Y. S. Hong, M. S. Kim, H. R. Cho, T. Kang, K. Shin, S. H. Choi, T. Hyeon, D.-H. Kim, Wearable/disposable sweat-based glucose monitoring device with multistage transdermal drug delivery module. *Sci. Adv.* **3**, e1601314 (2017).
3. W. Gao, S. Emaminejad, H. Y. Y. Nyein, S. Challa, K. Chen, A. Peck, H. M. Fahad, H. Ota, H. Shiraki, D. Kiriya, D.-H. Lien, G. A. Brooks, R. W. Davis, A. Javey, Fully integrated wearable sensor arrays for multiplexed *in situ* perspiration analysis. *Nature* **529**, 509–514 (2016).
4. H. Y. Y. Nyein, M. Bariya, L. Kivimäki, S. Uusitalo, T. S. Liaw, E. Jansson, C. H. Ahn, J. A. Hangasky, J. Zhao, Y. Lin, T. Happonen, M. Chao, C. Liedert, Y. Zhao, L.-C. Tai, J. Hiltunen, A. Javey, Regional and correlative sweat analysis using high-throughput microfluidic sensing patches toward decoding sweat. *Sci. Adv.* **5**, eaaw9906 (2019).
5. M. Bariya, H. Y. Y. Nyein, A. Javey, Wearable sweat sensors. *Nat. Electron.* **1**, 160–171 (2018).
6. A. Koh, D. Kang, Y. Xue, S. Lee, R. M. Pielak, J. Kim, T. Hwang, S. Min, A. Banks, P. Bastien, M. C. Manco, L. Wang, K. R. Ammann, K.-I. Jang, P. Won, S. Han, R. Ghaffari, U. Paik, M. J. Slepian, G. Balooch, Y. Huang, J. A. Rogers, A soft, wearable microfluidic device for the capture, storage, and colorimetric sensing of sweat. *Sci. Transl. Med.* **8**, 366ra165 (2016).
7. J. Kim, I. Jeerapan, S. Imani, T. N. Cho, A. Bandodkar, S. Cinti, P. P. Mercier, J. Wang, Noninvasive alcohol monitoring using a wearable tattoo-based iontophoretic-biosensing system. *ACS Sens.* **1**, 1011–1019 (2016).
8. Z. Sonner, E. Wilder, T. Gaillard, G. Kasting, J. Heikenfeld, Integrated sudomotor axon reflex sweat stimulation for continuous sweat analyte analysis with individuals at rest. *Lab Chip* **17**, 2550–2560 (2017).

9. Y. Yang, Y. Song, X. Bo, J. Min, O. S. Pak, L. Zhu, M. Wang, J. Tu, A. Kogan, H. Zhang, T. K. Hsiai, Z. Li, W. Gao, A laser-engraved wearable sensor for sensitive detection of uric acid and tyrosine in sweat. *Nat. Biotechnol.* **38**, 217–224 (2020).
10. A. Hauke, P. Simmers, Y. R. Ojha, B. D. Cameron, R. Ballweg, T. Zhang, N. Twine, M. Brothers, E. Gomez, J. Heikenfeld, Complete validation of a continuous and blood-correlated sweat biosensing device with integrated sweat stimulation. *Lab Chip* **18**, 3750–3759 (2018).
11. P. Simmers, S. K. Li, G. Kasting, J. Heikenfeld, Prolonged and localized sweat stimulation by iontophoretic delivery of the slowly-metabolized cholinergic agent carbachol. *J. Dermatol. Sci.* **89**, 40–51 (2018).
12. A. Martín, J. Kim, J. F. Kurniawan, J. R. Sempionatto, J. R. Moreto, G. Tang, A. S. Campbell, A. Shin, M. Y. Lee, X. Liu, J. Wang, Epidermal microfluidic electrochemical detection system: Enhanced sweat sampling and metabolite detection. *ACS Sens.* **2**, 1860–1868 (2017).
13. A. Alizadeh, A. Burns, R. Lenigk, R. Gettings, J. Ashe, A. Porter, M. McCaul, R. Barrett, D. Diamond, P. White, P. Skeath, M. Tomczak, A wearable patch for continuous monitoring of sweat electrolytes during exertion. *Lab Chip* **18**, 2632–2641 (2018).
14. Y. Zhang, H. Guo, S. B. Kim, Y. Wu, D. Ostojich, S. H. Park, X. Wang, Z. Weng, R. Li, A. J. Bandodkar, Y. Sekine, J. Choi, S. Xu, S. Quaggin, R. Ghaffari, J. A. Rogers, Passive sweat collection and colorimetric analysis of biomarkers relevant to kidney disorders using a soft microfluidic system. *Lab Chip* **19**, 1545–1555 (2019).
15. A. J. Bandodkar, P. Gutruf, J. Choi, K. H. Lee, Y. Sekine, J. T. Reeder, W. J. Jeang, A. J. Aranyosi, S. P. Lee, J. B. Model, R. Ghaffari, C.-J. Su, J. P. Leshock, T. Ray, A. Verrillo, K. Thomas, V. Krishnamurthi, S. Han, J. Kim, S. Krishnan, T. Hang, J. A. Rogers, Battery-free, skin-interfaced microfluidic/electronic systems for simultaneous electrochemical, colorimetric, and volumetric analysis of sweat. *Sci. Adv.* **5**, eaav3294 (2019).
16. Y. Hu, C. Converse, M. C. Lyons, W. H. Hsu, Neural control of sweat secretion: A review. *Br. J. Dermatol.* **178**, 1246–1256 (2018).
17. S. Emaminejad, W. Gao, E. Wu, Z. A. Davies, H. Y. Y. Nyein, S. Challa, S. P. Ryan, H. M. Fahad, K. Chen, Z. Shahpar, S. Talebi, C. Milla, A. Javey, R. W. Davis, Autonomous sweat extraction and analysis applied to cystic fibrosis and glucose monitoring using a fully integrated wearable platform. *Proc. Natl. Acad. Sci. U.S.A.* **114**, 4625–4630 (2017).
18. Z. Sonner, E. Wilder, J. Heikenfeld, G. Kasting, F. Beyette, D. Swaile, F. Sherman, J. Joyce, J. Hagen, N. Kelley-Loughnane, R. Naik, The microfluidics of the eccrine sweat gland, including biomarker partitioning, transport, and biosensing implications. *Biomicrofluidics* **9**, 031301 (2015).
19. S. Lin, B. Wang, Y. Zhao, R. Shih, X. Cheng, W. Yu, H. Hojaiji, H. Lin, C. Hoffman, D. Ly, J. Tan, Y. Chen, D. D. Carlo, C. Milla, S. Emaminejad, Natural perspiration sampling and in situ electrochemical analysis with hydrogel micropatches for user-identifiable and wireless chemo/biosensing. *ACS Sens.* **5**, 93–102 (2020).
20. J. Kim, A. S. Campbell, B. E.-F. de Ávila, J. Wang, Wearable biosensors for healthcare monitoring. *Nat. Biotechnol.* **37**, 389–406 (2019).
21. A. Jajack, M. Brothers, G. Kasting, J. Heikenfeld, Enhancing glucose flux into sweat by increasing paracellular permeability of the sweat gland. *PLOS ONE* **13**, e0200009 (2018).
22. N. A. S. Taylor, C. A. Machado-Moreira, Regional variations in transepidermal water loss, eccrine sweat gland density, sweat secretion rates and electrolyte composition in resting and exercising humans. *Extrem. Physiol. Med.* **2**, 4 (2013).
23. K. J. Collins, F. Sargent, J. S. Weiner, Excitation and depression of eccrine sweat glands by acetylcholine, acetyl-β-methylcholine and adrenaline. *J. Physiol.* **148**, 592–614 (1959).
24. J. S. Weiner, The regional distribution of sweating. *J. Physiol.* **104**, 32–40 (1945).
25. G. Tashiro, M. Wada, M. Sakurai, A bromphenol blue method for visualizing sweat at the openings of the sweat ducts. *J. Invest. Dermatol.* **36**, 3–4 (1961).
26. D. Gagnon, M. S. Ganio, R. A. I. Lucas, J. Pearson, C. G. Crandall, G. P. Kenny, Modified iodine-paper technique for the standardized determination of sweat gland activation. *J. Appl. Physiol.* **112**, 1419–1425 (2012).
27. P. U. Giacomoni, T. Mammone, M. Teri, Gender-linked differences in human skin. *J. Dermatol. Sci.* **55**, 144–149 (2009).
28. E. A. Arens, H. Zhang, From Thermal and Moisture Transport in Fibrous Materials, in *The Skin's Role In Human Thermoregulation And Comfort*, N. Pan, P. Gibson, Eds. (Woodhead Publishing Limited, 2006).
29. D. B. Frewin, J. A. Downey, Sweating-physiology and pathophysiology. *Aust. J. Dermatol.* **17**, 82–86 (1976).
30. E. H. Wissler, 'Sweating', in *Human Temperature Control: A Quantitative Approach*, E. H. Wissler, Ed. (Springer, 2018), pp. 197–237.
31. M. J. Buono, Sweat ethanol concentrations are highly correlated with co-existing blood values in humans. *Exp. Physiol.* **84**, 401–404 (1999).
32. J. R. Cohn, E. A. Emmett, The excretion of trace metals in human sweat. *Ann. Clin. Lab. Sci.* **8**, 270–275 (1978).
33. W. Gao, H. Y. Y. Nyein, Z. Shahpar, H. M. Fahad, K. Chen, S. Emaminejad, Y. Gao, L.-C. Tai, H. Ota, E. Wu, J. Bullock, Y. Zeng, D.-H. Lien, A. Javey, Wearable microsensor array for multiplexed heavy metal monitoring of body fluids. *ACS Sens.* **1**, 866–874 (2016).
34. E. H. Fishberg, W. Bierman, Acid-base balance in sweat. *J. Biol. Chem.* **97**, 433–441 (1932).
35. M. J. Patterson, S. D. R. Galloway, M. A. Nimmo, Effect of induced metabolic alkalosis on sweat composition in men. *Acta Physiol. Scand.* **174**, 41–46 (2002).
36. A. Bhide, S. Muthukumar, A. Saini, S. Prasad, Simultaneous lancet-free monitoring of alcohol and glucose from low-volumes of perspired human sweat. *Sci. Rep.* **8**, 6507 (2018).
37. M. Gamella, S. Campuzano, J. Manso, G. González de Rivera, F. López-Colino, A. J. Reviejo, J. M. Pingarrón, A novel non-invasive electrochemical biosensing device for in situ determination of the alcohol content in blood by monitoring ethanol in sweat. *Anal. Chim. Acta* **806**, 1–7 (2014).
38. H. Y. Y. Nyein, W. Gao, Z. Shahpar, S. Emaminejad, S. Challa, K. Chen, H. M. Fahad, L.-C. Tai, H. Ota, R. W. Davis, A. Javey, A wearable electrochemical platform for noninvasive simultaneous monitoring of Ca^{2+} and pH. *ACS Nano* **10**, 7216–7224 (2016).
39. J. B. Shields, B. C. Johnson, T. S. Hamilton, H. H. Mitchell, The excretion of ascorbic acid and dehydroascorbic acid in sweat and urine under different environmental conditions. *J. Biol. Chem.* **161**, 351–356 (1945).
40. S. J. Padayatty, H. Sun, Y. Wang, H. D. Riordan, S. M. Hewitt, A. Katz, R. A. Wesley, M. Levine, Vitamin C pharmacokinetics: Implications for oral and intravenous use. *Ann. Intern. Med.* **140**, 533–537 (2004).
41. J. Zhao, H. Y. Y. Nyein, L. Hou, Y. Lin, M. Bariya, C. H. Ahn, W. Ji, A. Javey, Wearable Nutrition Tracker. Manuscript submitted for publication.
42. M. D. Fisher, V. R. Reddy, F. M. Williams, K. Y. Lin, J. G. Thacker, R. F. Edlich, Biomechanical performance of powder-free examination gloves. *J. Emerg. Med.* **17**, 1011–1018 (1999).
43. S. P. Lacour, D. Chan, S. Wagner, T. Li, Z. Suo, Mechanisms of reversible stretchability of thin metal films on elastomeric substrates. *Appl. Phys. Lett.* **88**, 204103 (2006).
44. T. Adrega, S. P. Lacour, Stretchable gold conductors embedded in PDMS and patterned by photolithography: Fabrication and electromechanical characterization. *J. Micromech. Microeng.* **20**, 055025 (2010).
45. J. R. Windmiller, J. Wang, Wearable electrochemical sensors and biosensors: A review. *Electroanalysis* **25**, 29–46 (2013).
46. M.-C. Chuang, Y.-L. Yang, T.-F. Tseng, T. Chou, S.-L. Lou, J. Wang, Flexible thick-film glucose biosensor: Influence of mechanical bending on the performance. *Talanta* **81**, 15–19 (2010).
47. J. Cai, K. Cizek, B. Long, K. McAferty, C. G. Campbell, D. R. Allee, B. D. Vogt, J. L. Belle, J. Wang, Flexible thick-film electrochemical sensors: Impact of mechanical bending and stress on the electrochemical behavior. *Sens. Actuat B-Chem* **137**, 379–385 (2009).
48. L. Z. Benet, D. Kroetz, L. Sheiner, J. Hardman, L. Limbird, Pharmacokinetics: The dynamics of drug absorption, distribution, metabolism, and elimination. *Goodman Gilman's Pharmacol. Basis Ther.* **3**, e27 (1996).
49. L.-C. Tai, W. Gao, M. Chao, M. Bariya, Q. P. Ngo, Z. Shahpar, H. Y. Y. Nyein, H. Park, J. Sun, Y. Jung, E. Wu, H. M. Fahad, D.-H. Lien, H. Ota, G. Cho, A. Javey, Methylxanthine drug monitoring with wearable sweat sensors. *Adv. Mater.* **30**, e1707442 (2018).
50. L.-C. Tai, T. S. Liaw, Y. Lin, H. Y. Y. Nyein, M. Bariya, W. Ji, M. Hettick, C. Zhao, J. Zhao, L. Hou, Z. Yuan, Z. Fan, A. Javey, Wearable sweat band for noninvasive levodopa monitoring. *Nano Lett.* **19**, 6346–6351 (2019).
51. Y. Lin, M. Bariya, H. Y. Y. Nyein, L. Kivimäki, S. Uusitalo, E. Jansson, W. Ji, Z. Yuan, T. Happonen, C. Liedert, J. Hiltunen, Z. Fan, A. Javey, Porous enzymatic membrane for nanotextured glucose sweat sensors with high stability toward reliable noninvasive health monitoring. *Adv. Funct. Mater.* **29**, 1902521 (2019).

Acknowledgments: We acknowledge M.B. for illustration/schematics in Fig. 1. **Funding:** This work was supported by the NSF Nanomanufacturing Systems for Mobile Computing and Mobile Energy Technologies (NASCENT), the Berkeley Sensor and Actuator Center (BSAC), and the Bakar fellowship. **Author contributions:** M.B., L.L., and A.J. conceived of the project, designed the experiment, and interpreted the results. M.B. and L.L. conducted the experiments, with assistance from H.Y.Y.N. and L.-C.T. R.G. contributed to sweat gland imaging, while C.H.A. assisted with sensor fabrication. **Competing interests:** The authors declare that they have no competing interest. **Data and materials availability:** All data needed to evaluate the conclusions in the paper are present in the paper and/or the Supplementary Materials. Additional data related to this paper may be requested from the authors.

Submitted 23 March 2020
Accepted 15 July 2020
Published 28 August 2020
10.1126/sciadv.abb8308

Citation: M. Bariya, L. Li, R. Ghattamaneni, C. H. Ahn, H. Y. Y. Nyein, L.-C. Tai, A. Javey, Glove-based sensors for multimodal monitoring of natural sweat. *Sci. Adv.* **6**, eabb8308 (2020).

Science Advances

Glove-based sensors for multimodal monitoring of natural sweat

Mallika Bariya, Lu Li, Rahul Ghattamaneni, Christine Heera Ahn, Hnin Yin Yin Nyein, Li-Chia Tai and Ali Javey

Sci Adv **6** (35), eabb8308.
DOI: 10.1126/sciadv.abb8308